DOI: 10.13009/EUCASS2019-514

Experimental Study on Jet Acoustics of Subscale Rocket Nozzles with a Different Divergent Contour Design

Ralf Stark, Dirk Schneider, Jan Martin and Stephan General
German Aerospace Center
Langer Grund, D-74239 Lampoldshausen, Germany

Abstract

To design launch pads and test facilities properly it is necessary to predict the noise emission of rocket engines as well as specific exhaust jet created tones. As existing prediction models are limited to jet engines with low jet Mach numbers, tests were performed to study the application in rocket engines with significant higher jet Mach numbers. Two subscale rocket nozzles were tested, differing in the contour type and the related exhaust jet shock pattern. The tests reveal several prominent tones of different types that appear only during fully-attached flow state.

1. Introduction

The noise emission of the rocket engine exhaust jet is crucial not only for the rocket and its payload itself but also for the launch pads and the test facilities with its public environment. Therefore, for the design and the subsequent approval process of the launch pads and the test facilities, it is necessary to predict the broadband noise emissions as well as specific jet created tones. To reduce the noise emission typically guiding tubes are used where a certain amount of water is injected. To design the guiding tube and its position properly the exhaust jets acoustical characteristics have to be understood first.

A lot of work has been performed on broadband noise emission of jet engine exhaust jets [1, 2], jet related specific tones [3, 4] and the interaction with guiding tubes [5]. All illustrate the location of the noise origin and the noise propagation are related to the exhaust jet shock pattern and the shear layer shape. Unfortunately, the predictions of noise emissions found in the literature are limited to jet Mach numbers up to $M_j = 2$ and temperature ratios up to $T_0/T_a = 4$, whereas rocket engines feature exhaust jet Mach numbers above $M_j > 3$ and temperature ratios above $T_0/T_a > 11$. It is questionable whether the reported jet engine findings can be directly assigned to rocket engines. For this reason, the DLR conducted tests to extend the existing literature data base and to generate validation data for numerical simulations [6, 7].

2. Experimental setup

The study was conducted at DLR's subscale test facility P6.2 in Lampoldshausen. Figure 1, left gives the facility flow chart with its 20 MPa vessels on the left, where dry gaseous nitrogen is stored under ambient temperature. A feeding system, consisting of an automatic valve, a filter, a pressure reducer, a regulation valve, and a mass flow meter, connects the fluid supply with a settling chamber that is mounted on a horizontal rig. The settling chamber is equipped with a set of grids and honeycombs to homogenize the flow. The mesh size is 4 mm², reducing the effective cross section down to 64%. The tested nozzle specimens were mounted downstream of the settling chamber (Fig. 1, right). The facility features a maximum total pressure of $p_0 = 6$ MPa with a maximum mass flow of 4.2 kg/s. Dry nitrogen is used as working fluid to avoid condensation effects (H_2O, CO_2, O_2, etc.).

DOI: 10.13009/EUCASS2019-514

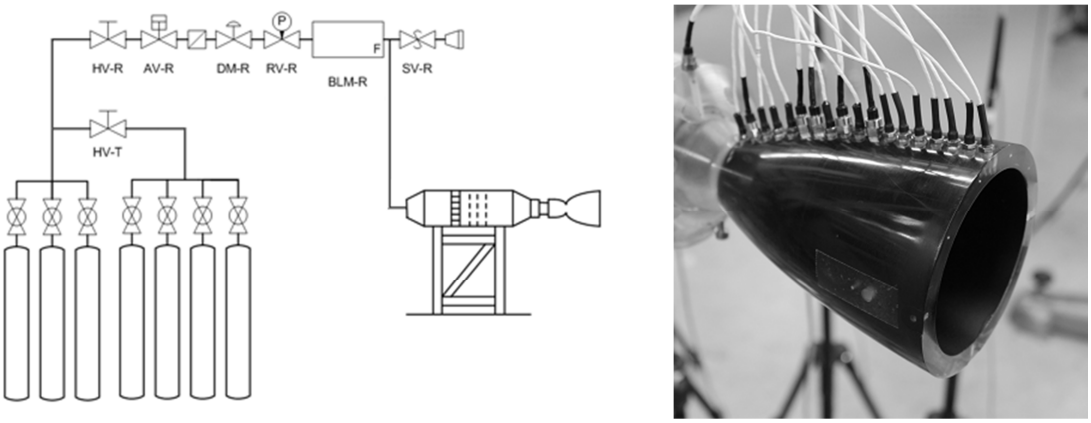

Figure 1: Flow chart of test facility P6.2, left and DLR-TIC on horizontal test rig, right

2.1 Test specimens, instrumentation and test sequences

To study the acoustical emissions of subscale rocket nozzles a thrust optimized parabola contour nozzle (TOP) and a truncated ideal contour nozzle (TIC) were chosen. In contrast, the TIC nozzle features a classical Mach disc pattern (Fig. 2, left), where the TOP nozzle features an internal shock that merges into a cap shock pattern (Fig. 2, right).

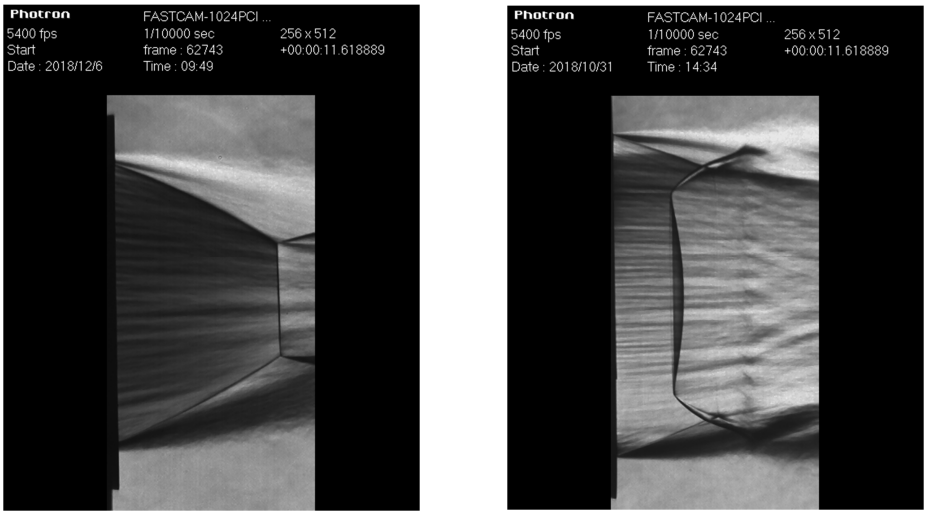

Figure 2: Exhaust jet shock pattern, DLR-TIC nozzle, left and DLR-S1 nozzle, right

Representative of the TOP nozzle, the DLR-S1 was selected. The DLR-S1 is a redesign of Östlund's S1 [8] cold flow subscale TOP nozzle which reliably produces a restricted shock separation (RSS) during start-up and shutdown [9].

The nozzle is equipped with 3 axial rows of pressure ports (Fig. 4, left). To measure the static wall pressure, orifices with a diameter of 0.0005 m are drilled perpendicular into the nozzle wall. The pressure ports are connected from small metal and Teflon tubes to blocks of pressure transducers. In total, 34 piezoresistive XT-154-190M type Kulite transducers are used. The transducers have a measurement range of 0.1 MPa with an accuracy of 0.5% relative to the upper range limit. The natural frequency of the transducers pressure sensitive semiconductor membrane is higher than 50 kHz. However due to the low eigenfrequency of the Teflon tubes, the pressure signals were filtered with a cut-off frequency of 160 Hz and recorded with a low frequency rate of 1 kHz.

To represent the TIC nozzle type, the standard DLR-TIC [10, 11] was selected, which features sufficiently comparable nozzle exit characteristics (Table 1). In addition, the DLR-TIC offers the possibility to mount 18 of the Kulite transducers directly into the nozzle wall (Fig. 1, right). Thus, high frequency measurements become feasible, with a sampling rate of 25 kHz and a cut-off filtering of 8 kHz. Both nozzles are made of acrylic glass.

Figure 3 gives the common test sequence of the TIC, left and the S1, right. Nearly the same maximum nozzle pressure ratios NPR = p_0/p_a and slopes were achieved. In contrast, the TIC features a fully attached flow regime for

DOI: 10.13009/EUCASS2019-514

NPR > 44, with no hysteresis behaviour for start-up and shutdown, where the S1 features in addition the RSS regime where the flow reattaches to the wall. The RSS range differs for start-up and shutdown. All flow regime transitions are marked with dashed lines.

Table 1: Nozzle characteristics

		DLR-TIC	**DLR-S1**
Design Mach number	M_D	5.15	6.78
Nozzle throat radius, m	R_t	0.01	0.011
Nozzle exit diameter, m	D_e	0.0905	0.098
Exit wall Mach number	M_e	4.38	4.43
Exit wall angle, °	α_e	5.3	4.7
Area ratio	ε	20.48	19.84
Internal shock		no	yes

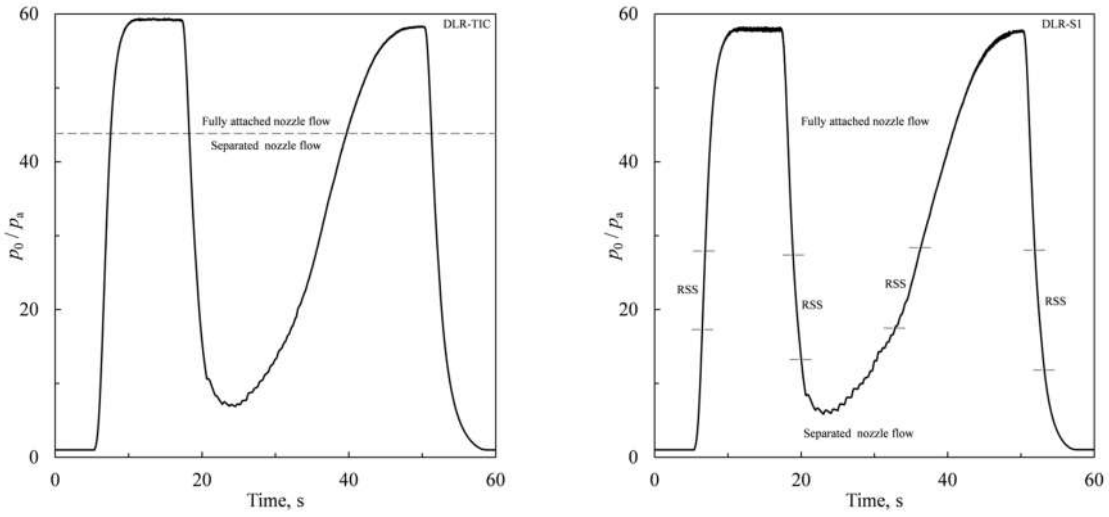

Figure 3: Test sequences, including flow regimes. DLR-TIC, left and DLR-S1, right

2.2 Acoustical and optical measurements

The acoustical emissions of the exhaust jets were measured using an array of 11 Brüel&Kjær type 4941 microphones (Fig. 4, left). The microphone array was connected to BK type LAN-XI 3050 modules, arranged in a mobile LAN-XI frame system. The array consisted of a line of 7 microphones aligned in parallel to the jet axis, in combination with 4 microphones mounted nearby the nozzle and the settling chamber. In this way the upstream and downstream noise propagation could be detected. The microphone positions were kept constant for both the TIC and the S1. Figure 4, right gives the effective microphone positions as well as a predefined virtual acoustical source at the nozzle exit and the out of it derived virtual microphones sphere with a diameter of $D_{vs} = 2.73$ m. In case of the TIC tests the microphone signals were scanned with a rate of 16.384 kHz, and in case of the S1 tests with a rate of 8.192 kHz. Digital filters of 6.4 kHz and 3.2 kHz were applied respectively.

DOI: 10.13009/EUCASS2019-514

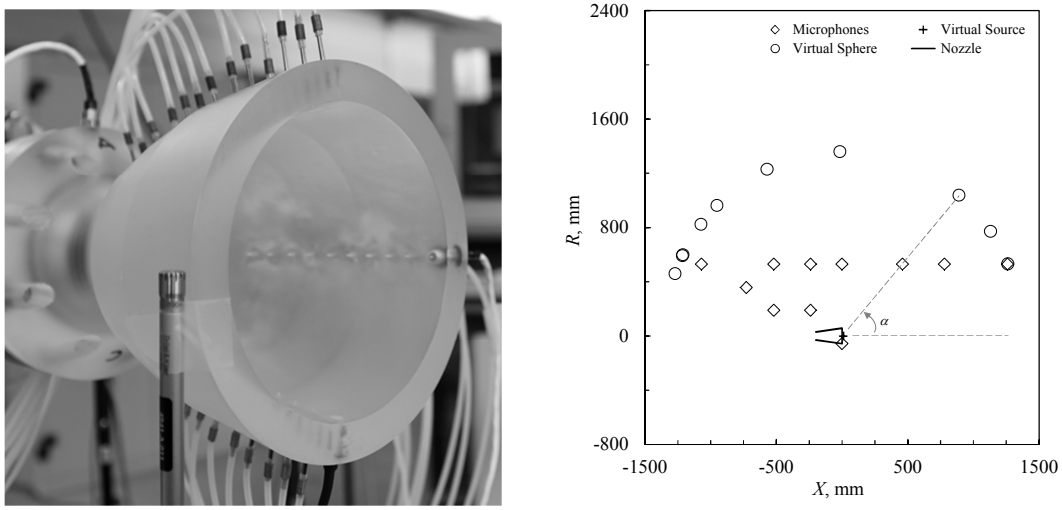

Figure 4: B&K type 4941 microphone nearby the DLR-S1 nozzle exit, left and positions of aligned microphones, virtual source and derived virtual sphere, right

The shock pattern of the nozzle exhaust jets were visualized with a classical b/w schlieren setting in z-formation [11]. The schlieren images were obtained with a frequency of 5400 fps, using a Photron Fastcam-1024PCI high speed camera system (Fig. 2). Subsequently, the resulting images were evaluated with an in-house DMD analysis code [12, 13].

3. Results and discussion

The TIC and the S1 were tested under same NPR conditions with identical acoustical and optical instrumentation to ensure the comparability of the experimental results.
Figure 5, left gives the overall sound pressure of the TIC as a function of the NPR, applying the previously mentioned virtual sphere. As expected, the overall sound pressure increases with increasing NPR. Figure 5, right compares the TIC and the S1 at NPR = 58.3. Except the most downstream microphone position at $\alpha = 23°$ the TIC gives higher overall sound pressure values. For correct comparison, the TIC microphone signals within both graphs were resampled at the S1 acquisition rate.

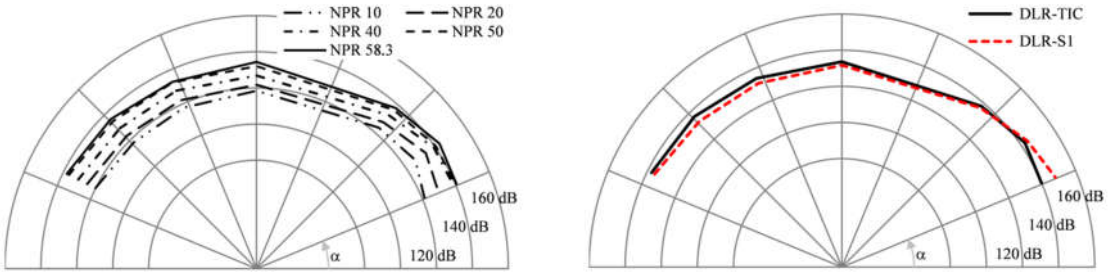

Figure 5: Overall sound pressure of DLR-TIC as function of nozzle pressure ratio, left and comparison of DLR-TIC and DLR-S1, right

The source of the increased TIC levels in most of the directions can be found in Fig. 6, left. The TIC features a prominent, clearly audible tone of 1187 Hz. The amplitude of the tone decreases for downstream (low) angles. In opposite, the S1 features a prominent tone of 2121 Hz, whose amplitude increases for downstream (low) angles. Both nozzles display a comparable tone at 824 Hz and 828 Hz respectively with dedicated harmonics.

DOI: 10.13009/EUCASS2019-514

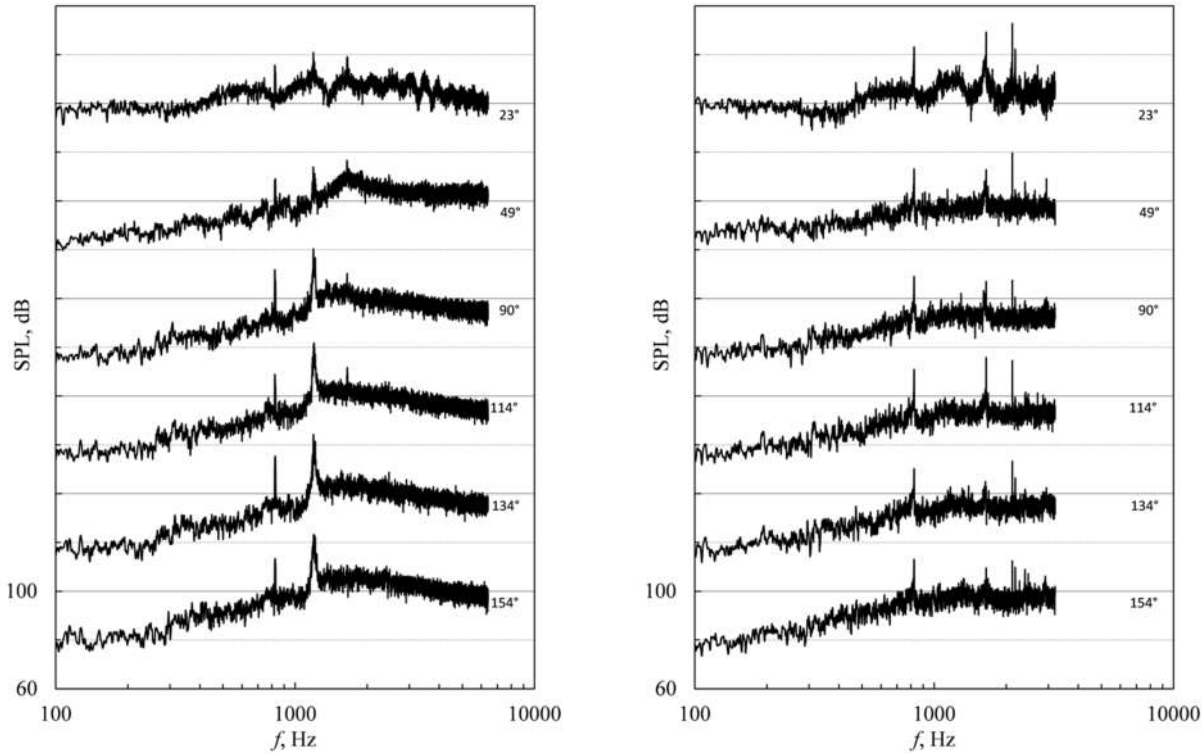

Figure 6: Sound pressure levels of DLR-TIC, left and DLR-S1, right at NPR = 58.3

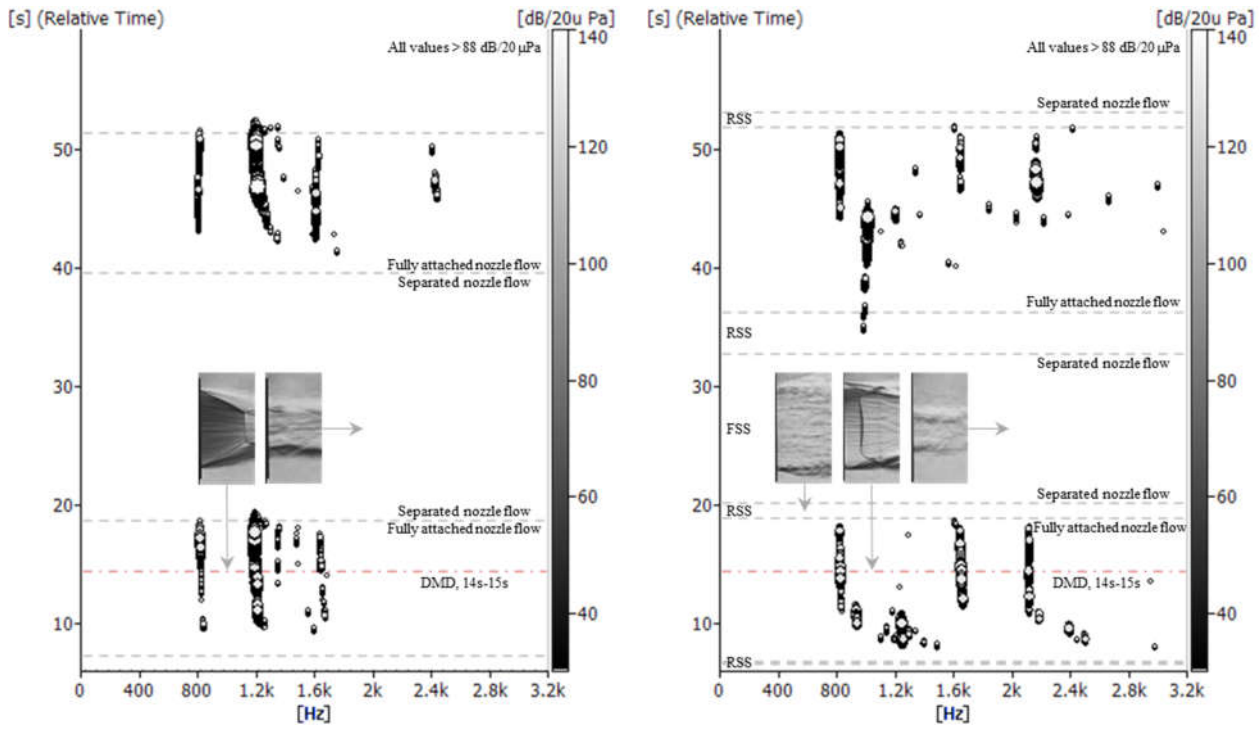

Figure 7: FFT vs. time of DLR-TIC, left and DLR-S1, right. Microphone position at 90°

DOI: 10.13009/EUCASS2019-514

A FFT analysis versus time (Fig. 7) reveals that for both nozzles the prominent tones only appear while the nozzle flow is fully attached and no separated backflow regions exist where ambient air is sucked into. The change from separated to fully-attached flow is marked with dashed lines in both graphs. The S1 additionally features during start-up and shutdown, the RSS flow state (Fig. 7, right), where the flow is redirected towards the nozzle wall and reattaches at the nozzle exit. The RSS condition is caused by an internal shock (see Fig. 9, left) that originates shortly downstream of the nozzle throat, and that creates in combination with the oblique separation shock, the cap shock pattern [10, 14]. To illustrate the different flow regimes, small instant schlieren images are added to the graphs. In addition, to increase the readability, a high pass amplitude filter of 88 dB was applied.
As the most prominent TIC tone appears while the nozzle is full-flowing, its frequency slightly decreases to 1187 Hz while the NPR increases. The frequency progress depicts a croissant shape. The S1 displays an additional tone of approximately 1000 Hz which appears during RSS while slowly up-ramping the NPR. Its frequency increases linearly. The tone disappears for high NPRs and is replaced by the prominent 828 Hz tone.

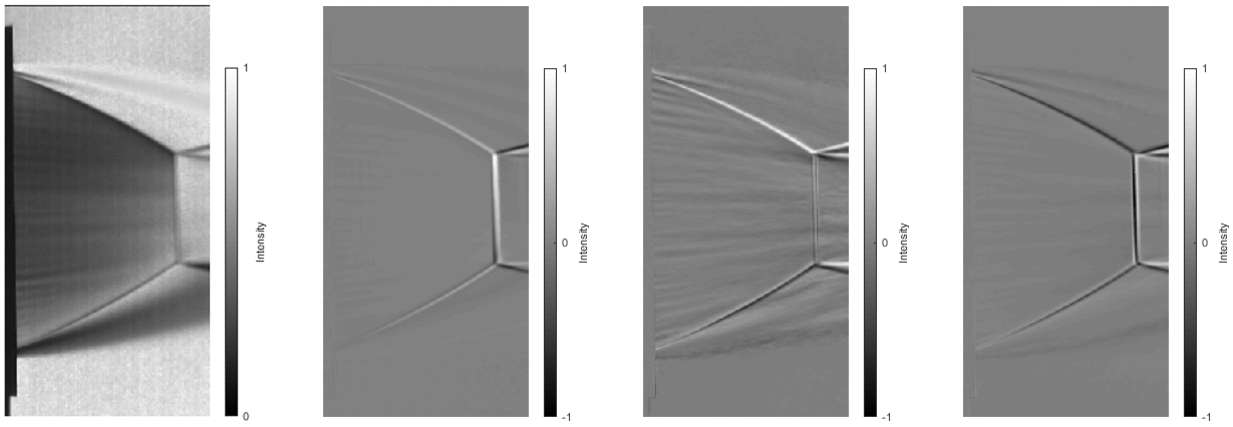

Figure 8: DMD of DLR-TIC, mean image, 824 Hz, 1187 Hz and 1648 Hz, from left to right

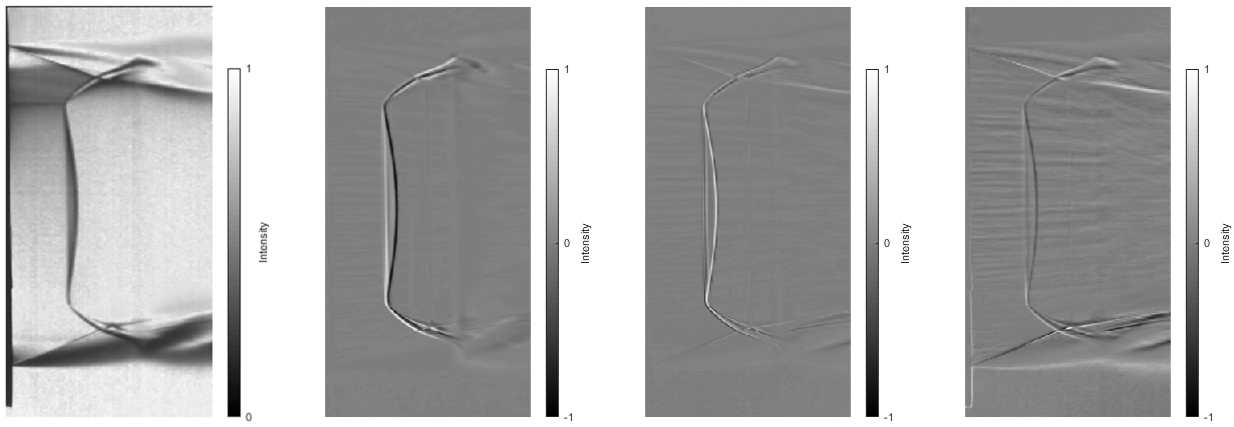

Figure 9: DMD of DLR-S1, mean image, 828 Hz, 1655 Hz and 2121 Hz, from left to right

To study the nature of the tones and the related exhaust jet pattern of the nozzles in detail, 5400 subsequent schlieren images underwent a DMD analysis, representing the time period of t = 14 to 15 s. The period is indicated as dot-dashed lines in Fig. 7.
Figure 8 presents the TIC results. The first image from the left displays the averaged mean intensity values. As the schlieren edge was oriented horizontally, density gradients of the oblique shocks appear as darkened in the upper part, and as brightened in the lower part. In contrast, expansions and shear layers appear vice versa. The successive images have to be interpreted differently: illustrated are the intensity changes for an explicit frequency mode, related to the mean image. The intensities are normalized by the corresponding maximum value and the images cannot be compared quantitatively. The second image from the left displays the 824 Hz mode. The oblique and reflected shocks appear with comparable intensities, whereas the Mach disc appears with mixed intensities. Hence, the shock

DOI: 10.13009/EUCASS2019-514

pattern identifies an axial piston mode. However, the third image, illustrating the 1187 Hz mode, is different. The oblique and reflected shocks are of opposite intensity, revealing a phase shift. The Mach disc is barely affected. As it is very unlikely that a nozzle reveals during all tests the same vertically fixed flapping mode, the shock pattern has to be interpreted as a rotational, almost certainly a helical, mode. In addition, the vortex structures of the shear layer are noticeable (see also Fig. 2, left). However, it has to be considered that the absolute intensity of the third image is an order of magnitude below the absolute intensity of the second image. The fourth image illustrates the 1648 Hz harmonic.

Figure 9 presents the S1 results. From left to right: the averaged mean image, the 828 Hz mode, its harmonic, the 1655 Hz mode, and the 2121 Hz mode. The mean image exhibits the discussed internal shock much better than an instant schlieren image (Fig. 2, right). The DMD analysis reveals that the 828 Hz mode is likewise of an axial piston type, whereas the 2121 Hz mode is a rotational one. Its absolute intensity is an order of magnitude below the 828 Hz mode, as for the TIC case. Therefore, the shear layer vortices structure appears intensified as well.

Using the mean images, the oblique shock angles and the related recompression can be determined. The derived exhaust jet characteristics downstream the oblique shocks and a comparison are presented in Table 2.

Table 2: Exhaust jet characteristics

		DLR-TIC	**DLR-S1**	**Ratio**
Exit wall Mach number	M_e	4.38	4.43	0.9987
Oblique shock angle, °	σ	26.1	24.2	1.0785
Jet Mach number	M_j	3.11	3.29	0.9453
Pressure reduction, %	p_{02}/p_{01}	75.8	80.8	0.9381
Jet pressure ratio	p_j/p_a	1.054	0.854	1.2342
Jet velocity, m/s	u_j	606.9	640.6	0.9474
Temperature ratio	T_0/T_a	0.9965	0.9795	1.0174
Nozzle exit diameter, m	D_e	0.0905	0.098	0.9235
Ratio diameter/velocity, s	D_e/u_j	$1.491 \cdot 10^{-4}$	$1.529 \cdot 10^{-4}$	0.9751
Frequency prediction, Hz	f_{TSY}	681	622	1.0948
Jet Mach number, isentropic	M_{jisen}	3.34	3.32	1.0060

Applying the obtained jet velocities u_j and the nozzle exit diameters D_e, respectively, the measured frequencies f can be converted to Strouhal numbers $St = f \cdot D_e/u_j$. Figure 10 illustrates the sound pressure levels (SPL) of the TIC (left) and the S1 (right) as function of the Strouhal number. Whereas the TIC's prominent tone (rotational mode) of $f = 1187$ Hz turns into a Strouhal number of $St = 0.18$, the S1's prominent tone (rotational mode) of $f = 2121$ Hz turns into $St = 0.32$. Although the nozzle exit diameters and jet velocities differ clearly, the derived diameter to jet velocity ratios D_e/u_j are close (Tab. 2). Therefore, the Strouhal numbers of the TIC's prominent tone of $f = 824$ Hz (piston mode) and the S1's prominent tone of $f = 828$ Hz turn into close Strouhal numbers of $St = 0.123$ and $St = 0.126$, respectively. Disregarding all prominent tones, in both cases, the maximum SPL appear at Strouhal numbers of approximately $St \sim 0.2$.

$$\frac{f D_j}{u_j} = 0.67\left(M_j{}^2 - 1\right)^{-\frac{1}{2}}\left[1 + 0.7M_j\left(1 + \frac{\gamma_j - 1}{2}M_j{}^2\right)^{-\frac{1}{2}}\left(\frac{T_0}{T_a}\right)^{\frac{1}{2}}\right]^{-1} \quad (1)$$

DOI: 10.13009/EUCASS2019-514

$$M_{jisen} = \sqrt{\frac{2}{\gamma-1}\left[\left(\frac{p_0}{p_a}\right)^{\frac{\gamma-1}{\gamma}} - 1\right]} \tag{2}$$

Prominent tones can be predicted using e.g. the method of Tam et al. [3] (Eq. 1). The derived frequencies of the TIC $f_{\text{TSY-TIC}}$ = 681 Hz and the S1 $f_{\text{TSY-S1}}$ = 622 Hz do not match with any prominent tone. Using the simply determined isentropic jet Mach numbers (Eq. 2) does not improve the prediction distinctly.

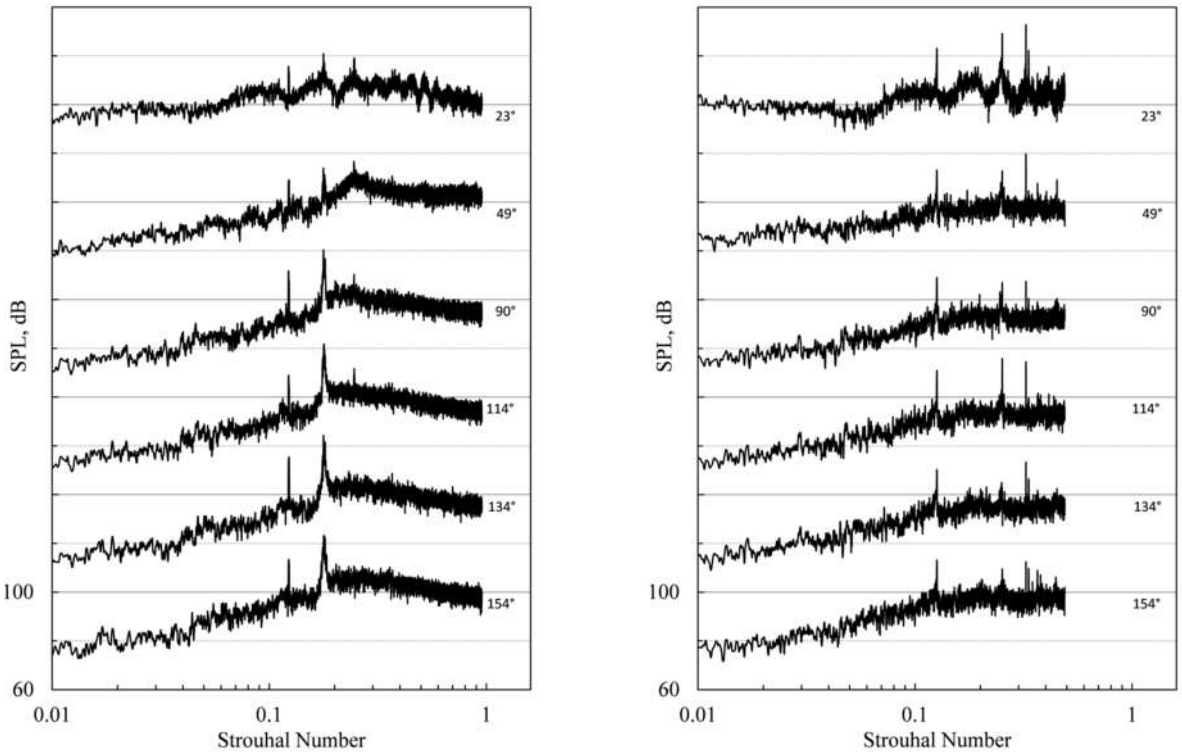

Figure 10: Sound pressure levels as function of Strouhal number. DLR-TIC, left and DLR-S1, right at NPR = 58.3

4. Conclusion

In this study, a truncated ideal contour nozzle and a thrust optimized parabola nozzle were compared. The exhaust jet shock pattern could be correlated with the associated acoustical emissions. Incourse of the analysis, some principal conclusions could be drawn.

In both cases, the prominent tones only appear if the nozzles are full-flowing, i.e. no separated back flow regions exist, where ambient air is sucked into. The free fluctuating flow separation seems to disturb the production of distinct tones. In contrast, fixed flow separations, e.g. by means of edges, support the production of tones.

The nozzles reveal a prominent tone and its harmonic with comparable frequencies and Strouhal numbers. The tone is an axial piston type mode. As the nozzles feature comparable flow properties upstream the recompressing shock pattern and nearly equal subsonic inflow conditions, it is very likely that a common source is located within the undisturbed nozzle flow.

The TIC and the S1 feature prominent rotational modes of different frequencies. As the nozzle's exhaust jets strongly differ concerning the size and the shape of the shear layer, the shock pattern, and the subsonic core downstream the Mach disc (TIC) and the cap shock (S1), the source of these tones must be located downstream the shock systems.

The frequencies of the prominent tones could not be predicted.

DOI: 10.13009/EUCASS2019-514

Acknowledgements

The authors like to thank M. Razavi (University of Toronto) for enhancing the DMD routines. The present work was conducted in the framework of the German Aerospace Center (DLR) project TAUROS (TAU for Rocket Thrust Chamber Simulation) focusing on the qualification and advancement of the DLR flow solver TAU for liquid rocket thrust chamber applications. The financial support of the DLR Space Research Programmatic is highly appreciated.

References

[1] Tam C. and L. Auriault. 1999. Jet Mixing Noise from Fine-Scale Turbulence. *AIAA Journal*, Vol. 37, pp. 145-153.

[2] Kandula M. 2008. Shock-Refracted Acoustic Wave Model for Screech Amplitude in Supersonic Jets. *AIAA Journal*, Vol. 46, No. 3, pp. 682-689.

[3] Tam C., J. Seiner and J. Yu. 1986. Proposed Relationship between Broadband Shock Associated noise and screech Tones. *Journal of Sound and Vibrations*, 110(2), pp 309-321.

[4] Tinney C.E., P. Panickar and P. Vogel. 2018. Aeroacoustics of a Planar Multistream Supersonic Nozzle with Aft Deck and Sidewalls. *AIAA Journal*, Vol. 56, No. 10, pp. 3926-3937.

[5] Sebourn C. L. and F. L. Shope. 2005. Research Summary on the AEDC ASTF C-2 Aeroacoustic Resonance Phenomenon. AIAA2005-2932, Monterey.

[6] Costa Ruiz E., R. Stark and S. General. 2019. Prediction of Subscale Rocket Engine Acoustic Emissions Using CAA Hybrid Methods. EUCASS, 8th European Conference for Aerospace Sciences, No. 613, 1-4 July, Madrid, Spain.

[7] Costa Ruiz E., S. General, R. Stark, F. Strauss and D. Schneider. Numerical Analysis of a Quadratic Supersonic Jet using CAA-Hybrid Methods. 55th AIAA/ASME/SAE/ASEE Joint Propulsion Conference, 19-22 August, Indianapolis, Indiana.

[8] Östlund J. 2004. Supersonic flow separation with application to rocket engine nozzles. PhD Thesis, Royal Institute of Technology, Stockholm, Sweden,.

[9] Stark, R. and C. Génin. 2016. Optimisation of a Rocket Nozzle Side Load Reduction Device, *Journal of Propulsion and Power*, Vol. 32, No. 6, pp. 1395-1402.

[10] M. Frey. 2001. Behandlung von Strömungsproblemen in Raketendüsen bei Überexpansion. Ph.D. Thesis, Univ. Stuttgart, Germany, Shaker Verlag.

[11] R. Stark and B. Wagner. 2009. Experimental study of boundary layer separation in truncated ideal contour nozzles. *Shock Waves*, Vol. 19, No. 3, pp 185-191.

[12] Schmid P. J. 2010. Dynamic mode decomposition of numerical and experimental data. *Journal of Fluid Mechanics*, Vol. 656, pp. 5-28.

[13] Beinke S. K., J. Hardi, M. Oschwald, D. T. Banuti, S. Karl and B. B. Dally. 2018. Experimental and numerical study of oxygen-hydrogen rocket flame response to transverse acoustic excitation. AIAA Propulsion and Energy Forum. AIAA2018-4947.

[14] R. Stark. 2010. Beitrag zum Verständnis der Strömungsablösung in Raketendüsen. Ph.D. Thesis, RWTH Aachen, Germany.